

Emergent magnetic states due to stacking and strain in the van der Waals magnetic trilayer CrI₃

Zhen Zhang,¹ Jing-Yang You,^{2,*} Bo Gu,^{3,4,†} and Gang Su^{1,3,4,‡}

¹*School of Physical Sciences, University of Chinese Academy of Sciences, Beijing 100049, China*

²*Department of Physics, National University of Singapore, 2 Science Drive 3, 117551, Singapore*

³*Kavli Institute for Theoretical Sciences, and CAS Center for Excellence in Topological Quantum Computation, University of Chinese Academy of Sciences, Beijing 100190, China*

⁴*Physical Science Laboratory, Huairou National Comprehensive Science Center, Beijing 101400, China*

Recently, three different magnetic states were observed experimentally in trilayer CrI₃ under pressure, including ferromagnetic (FM)-↑↑↑, FM-↓↑↓ and FM-↑↑↓. To reveal the nature of the observed three magnetic states, we studied the magnetic properties of four possible stacking structures in trilayer CrI₃: I (rhombohedral), II (monoclinic), III (hexagonal) and IV (triclinic). We find that all four stacking structures possess the FM-↑↑↑ ground state. After applying a few strains, the FM-↓↑↓ becomes the ground state in II and III structures, and the FM-↑↑↓ is preferred in IV structure, while the FM-↑↑↑ persists in I structure. Our results unveil that the three magnetic states observed in trilayer CrI₃ may correspond to different stacking structures with small tensile strains, which can well interpret the experimentally obtained pressure dependent interlayer coupling and Curie temperature. Our present study paves a way to design the magnetic multilayers with required magnetic states by tuning stacking and strain.

I. INTRODUCTION

After the recent discovery of ferromagnetic order in atomically thin layer CrI₃ [1] and Cr₂Ge₂Te₆ [2], two-dimensional (2D) van der Waals (vdW) ferromagnetic semiconductors have attracted much attention due to their exotic properties and potential applications in spintronics[3–7]. According to Mermin-Wagner theorem [8], the large magnetic anisotropy is required to stabilize the long-range ferromagnetism in 2D materials [9–12].

The magnetism in 2D materials can be sensitively controlled by external perturbations, such as electric field [10, 13–15], strain [16, 17] and stacking [18]. The stacking engineering is very promising, because there are many possible compositions to construct heterostructures with different 2D materials to enhance the magnetic properties[19–22], and to produce novel physical phenomena, such as the quantum anomalous Hall effect [23, 24], and axion insulators [25].

The 2D CrI₃, as an Ising-type ferromagnets with the Curie temperature of 45K in monolayer, has become a highlighted research hotspot.[26–38]. For a few layers of CrI₃, it can be used as a spin-filter tunnel barrier possessing a giant tunneling magnetoresistance [26–29], and the magnetic interactions between adjacent layers can be tuned by electric gating, electrostatic doping and pressure[39–43]. Most of the theoretical studies on few-layers CrI₃ focused on bilayer [30–32, 35], and they show that rhombohedral stacking favors ferromagnetic (FM) interlayer interaction, while monoclinic stacking is beneficial to antiferromagnetic (AFM) interlayer interaction, which is in good agreement with the experimental observations[33]. Bulk CrI₃ is reported to be a ferromagnetic semiconductor with a band gap of about 1.2 eV [44], which maintains the rhombohedral stacking se-

quence with $R\bar{3}$ space group symmetry with the temperature lower than ~ 220 K, and transforms to the monoclinic stacking with $C2/m$ space group at higher temperature [45].

Recently, researchers have turned their attention to trilayer CrI₃. In 2019, Peng et al observed the rhombohedral stacking order with FM interlayer interaction (FM-↑↑↑) at 10K in non-encapsulated trilayer CrI₃ [34]. However, Xu et al reported that the pristine exfoliated trilayer CrI₃ favors AFM interlayer interaction with spin antiparallel arrangement of every two adjacent layers (labeled as ↓↑↓), and under pressures, three magnetic states, i.e. FM-↑↑↑, FM-↓↑↓, and FM-↑↑↓, can be obtained in trilayer CrI₃ [43]. It becomes important to uncover the nature of different magnetic states in trilayer CrI₃ observed in recent experiments.

In this paper, we systematically investigate the magnetic properties of the trilayer CrI₃ with four different stacking structures, including I (rhombohedral), II (monoclinic), III (hexagonal) and IV (triclinic). Our results show that the magnetic states FM-↑↑↑, FM-↓↑↓, and FM-↑↑↓ experimentally observed in trilayer CrI₃ may come from different stacking structures with small tensile strain in trilayer CrI₃. The correspondence between the stacking structure and interlayer magnetic coupling could provide us a basis to design spintronic devices with desirable magnetic properties by adjusting the stacking order and strains.

II. COMPUTATIONAL METHODS

In our calculations, the projector augmented wave (PAW) method [46] based on the density functional theory (DFT) as implemented in the Vienna ab initio simu-

lation package (VASP) [47, 48] is employed to carry out the first-principles calculations. The generalized gradient approximation (GGA) in the form proposed by Perdew, Burke, and Ernzerhof (PBE) [49] is used to describe the electron exchange-correlation functional. To simulate the quasi-2D materials, a sufficiently large vacuum of 15 Å along the z direction is built. The zero damping DFT-D3 method is adopted to describe the interlayer van der Waals interaction. The plane-wave cutoff energy is set to be 450 eV. Structural optimization including lattice constant and atomic positions is done with the conjugate gradient (CG) scheme until the maximum force acting on each atoms is less than 0.01 eV/Å and the total energy is converged to 10^{-5} eV. The $9 \times 9 \times 1$ k -point mesh grid within the first Brillouin zone [50] is used for structure optimization and self-consistent calculation. Self-consistent-field DFT calculations incorporating the spin-orbit coupling (SOC) are used to obtain the energies accurately. Considering the on-site Coulomb interaction of Cr $3d$ orbitals, $U = 3$ eV is used in all calculations, and the effect of different U values is also tested to show the robustness of our results.

III. RESULTS

A. Four stacking orders in trilayer CrI₃

The primitive cell of monolayer CrI₃ consists of two magnetic Cr atoms and six I atoms with each Cr atom surrounded by six I atoms forming a distorted octahedron. The basic vectors \mathbf{a} and \mathbf{b} are along the zigzag direction of the honeycomb lattice composed of Cr atoms and the y -axis corresponds to the armchair direction as shown in Fig. 1(a). Here, we consider four different stacking structures in trilayer CrI₃: I (rhombohedral), which is the low-temperature phase of bulk CrI₃ with the upper layer of two adjacent layers always translating $\sqrt{3}/3a$ in the armchair direction (y -axis) relative to the lower layer; II (monoclinic), the high-temperature phase of bulk CrI₃ with the upper layer of two adjacent layers always moving $1/3a$ in the zigzag (\mathbf{a}) direction relative to the lower layer; III (hexagonal), which is the primitive cell of the bulk CrI₃ with $P3_112$ space group, where the middle and top layers move $1/3a$ along the zigzag direction \mathbf{a} and \mathbf{b} directions relative to the lower layer, respectively; IV (triclinic), which is constructed with the middle and top layer moving $1/3a$ and $\sqrt{3}/3a$ along the zigzag (\mathbf{a}) and armchair (y) directions relative to the lower layer, respectively, as shown in Figs. 1(a)-(d).

To study the possible stacking structures of trilayer CrI₃, the interlayer exchange couplings are essential, which should be included in the model. Because the interlayer Cr-Cr distances (d'_1 , d'_2 and d'_3) are comparable with the intralayer second and third neighboring Cr-Cr distances (d_2 , d_3), as noted in Table S3 in Supplemental

TABLE I. Structural parameters for bulk and trilayer CrI₃. Lattice constant (a), interlayer distance (d_1 and d_2) reported in the experiment for bulk CrI₃ with rhombohedral and monoclinic stacking orders [45] and our DFT results for trilayer CrI₃ with I (rhombohedral), II(monoclinic), III (hexagonal) and IV (triclinic) stacking orders. d_1 and d_2 refer to the distance between the middle layer and its upper and lower layers, respectively, as shown in Fig. 1(a).

CrI ₃		a (Å)	d_1 (Å)	d_2 (Å)
Bulk (Exp. in[45])	rhombohedral	6.867	6.602	6.602
	monoclinic	6.866	6.623	6.623
Trilayer (DFT)	I(rhombohedral)	6.962	6.706	6.706
	II (monoclinic)	6.957	6.762	6.762
	III (hexagonal)	6.960	6.755	6.755
	IV (triclinic)	6.960	6.681	6.720

Materials, it is necessary to consider the intralayer second and third nearest-neighboring exchange couplings (J_2 and J_3). In order to explore the relation between magnetic states and stacking structures of trilayer CrI₃, for each stacking structure we have studied four magnetic states FM- $\uparrow\uparrow\uparrow$, FM- $\uparrow\uparrow\downarrow$, FM- $\downarrow\uparrow\downarrow$ and AFM in our calculations, where FM (AFM) and $\uparrow\uparrow\uparrow$ ($\uparrow\uparrow\downarrow$, $\downarrow\uparrow\downarrow$) represent the intralayer and interlayer exchange couplings, respectively, as shown in Fig. 1(e). By comparing the total energies of different spin configurations for every stacking structure, FM- $\uparrow\uparrow\uparrow$ state is found to be the magnetic ground state for the above four stacking structures, and the experimental and calculated structural parameters are listed in Table I. Among the four stacking structures, I (rhombohedral) stacking structure possesses the lowest energy, and we select its lattice constant 6.962 Å as the initial lattice constant to investigate the effect of in-plane strain.

For the mixture of rhombohedral and hexagonal stackings, it contains the relative movement between adjacent layers in both armchair and zigzag directions, which is identical to the IV (triclinic) stacking order. For the mixture of hexagonal and monoclinic stackings, it contains the relative movement between adjacent layers in the zigzag direction, leading to II (monoclinic) and III (hexagonal) stacking structures.

B. Magnetic ground state

For simplicity, we apply the in-plane biaxial strain to investigate the strain effect on magnetic properties in trilayer CrI₃ for four different stacking structures. The in-plane biaxial strain is defined as $\varepsilon = (a - a_0)/a_0$,

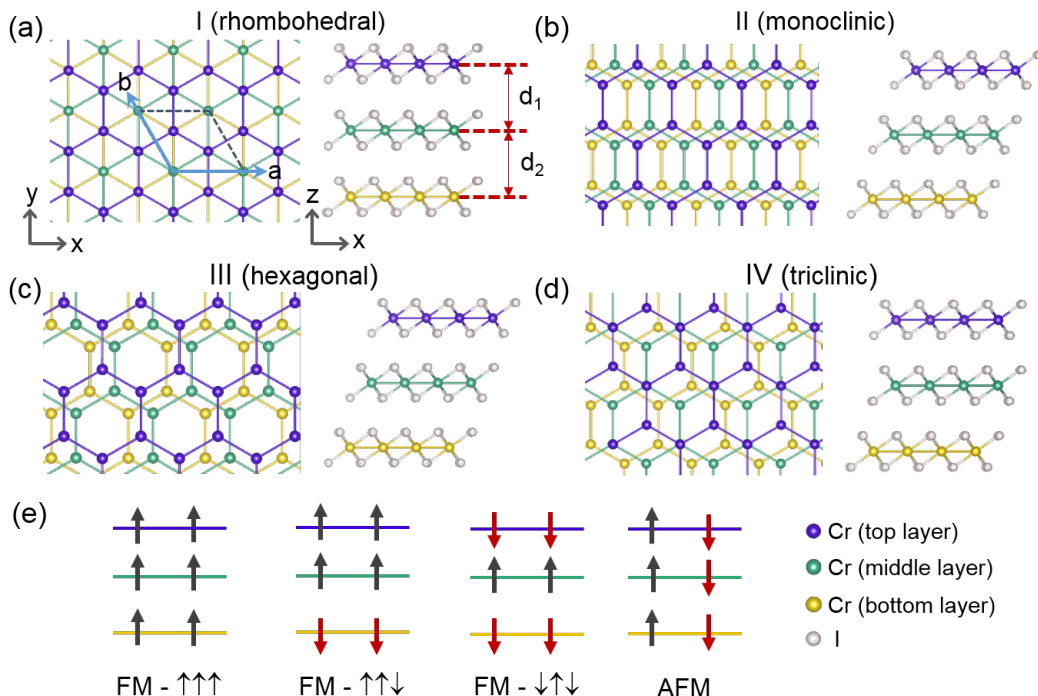


FIG. 1. The top and side views of (a) rhombohedral, (b) monoclinic, (c) hexagonal and (d) triclinic stacking structures in trilayer CrI_3 . The yellow, green, and purple balls are the bottom, middle, and top Cr layers, respectively. (e) Schematic plot of four different spin configurations. FM and AFM denote the ferromagnetic and antiferromagnetic intralayer exchange couplings, respectively, and $\uparrow\uparrow\uparrow$, $\uparrow\uparrow\downarrow$ and $\downarrow\uparrow\downarrow$ represent the three possible interlayer spin orientations.

where a_0 and a are lattice parameters without and with strain, respectively. For the trilayer CrI_3 with I (rhombohedral) stacking structure, the interlayer distance (d) decreases from 7.05 to 6.38 Å with the in-plane biaxial strain changing from -10% to 10% as shown in Fig. S1. With the increase of tensile strain, the FM- $\uparrow\uparrow\uparrow$ spin configuration is always the magnetic ground state, and the energy difference between other spin configurations and FM- $\uparrow\uparrow\uparrow$ is increased, indicating a more stable FM- $\uparrow\uparrow\uparrow$ magnetic state with the decrease of interlayer distance. While with the increase of compressive strain, a magnetic phase transition from FM- $\uparrow\uparrow\uparrow$ to AFM will occur when the compressive strain is larger than 6%. The similar magnetic phase transition from intralayer FM to AFM with the increase of compressive strain also occurred in monolayer CrI_3 [51]. For trilayer CrI_3 with II (monoclinic) and III (hexagonal) stacking structures, a tiny tensile strain will cause a magnetic phase transition from FM- $\uparrow\uparrow\uparrow$ to FM- $\downarrow\uparrow\downarrow$, and the reduced interlayer distance can stabilize the FM- $\downarrow\uparrow\downarrow$ state. The change of magnetic phases under compressive strain for II and III structures is similar to that for the I (rhombohedral) stacking structure. The above I, II, III stacking structures cannot lead to the FM- $\uparrow\uparrow\downarrow$ magnetic phase, which was observed in the experiment. To understand the stacking structure of the magnetic state FM- $\uparrow\uparrow\downarrow$, which involves the both ferromagnetic and antiferromagnetic interlayer couplings in

trilayer CrI_3 , we have considered the IV (triclinic) stacking structure, which combines the structures of I and II (or III). Therefore, three magnetic states FM- $\uparrow\uparrow\uparrow$, FM- $\downarrow\uparrow\downarrow$ and FM- $\uparrow\uparrow\downarrow$ observed experimentally in the trilayer CrI_3 [43] are all obtained in our calculations.

To study the relative stability of four stacking orders under different strains as shown in Fig. 2 (e), and find that in the range of compressive strain -6% to tensile strain 10%, the energy of the I (rhombohedral) stacking structure is always the lowest, and II (monoclinic) and III (hexagonal) structures have almost the same energy and is the highest. The total energy of the IV (triclinic) stacking structure is between that of I (rhombohedral) and II (monoclinic) structures, and it is interesting to note that the IV structure can be regarded as the combination of structures I and II. As shown in Fig. 2 (f), the electronic band gap shows a strong dependence on the magnetic states in trilayer CrI_3 . In the range of 0~-10% compressive strain, four stacking structures I to IV possess the same magnetic ground states, and their band gaps are basically the same, and they all undergo a transition from semiconductor to metal with compressive tensile about -10%. In the range of 0~10% tensile strain, the band gaps for stacking structures I-IV become different, and at the same time their magnetic ground states become different.

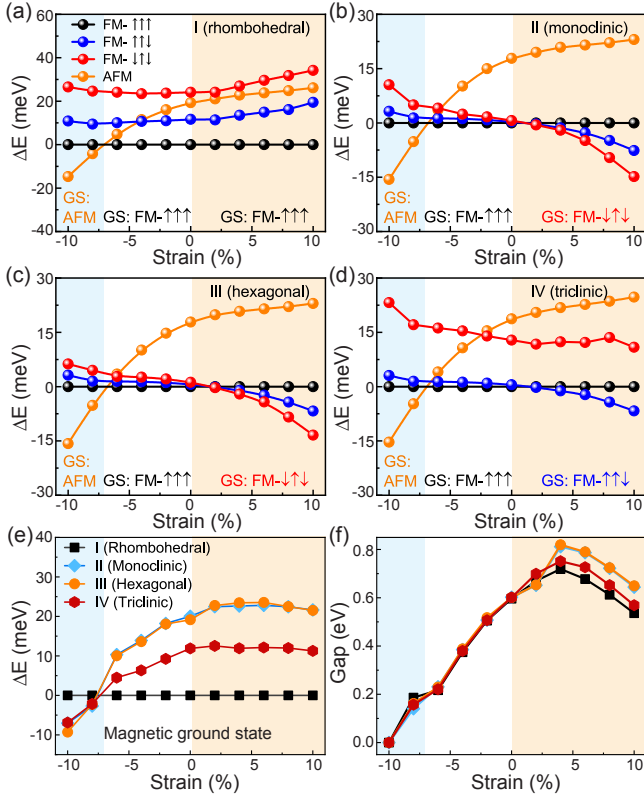


FIG. 2. The relative total energy as a function of strain for (a) rhombohedral, (b) monoclinic, (c) hexagonal and (d) triclinic stacking structures in trilayer CrI_3 . For every stacking order, four different spin configurations FM- $\uparrow\uparrow\uparrow$, FM- $\downarrow\uparrow\downarrow$, FM- $\uparrow\uparrow\downarrow$, and AFM are considered. The energy difference is defined as $\Delta E = E - E_0$, where E_0 is the energy of FM- $\uparrow\uparrow\uparrow$ state at corresponding strain. (e) The relative total energy of II, III and IV stacking structures. ΔE is defined as $\Delta E = E - E_I$, where E_I is the energy of I stacking structure under different strains. (f) Strain-dependent band gaps for four stacking structures in trilayer CrI_3 .

C. Theoretical model analysis

To better understand the relation between the magnetic states and the stacking structures in trilayer CrI_3 , we consider a Hamiltonian including intralayer and interlayer interactions $H = H_{intra} + H_{inter}$. The intralayer term H_{intra} is written as

$$H_{intra} = H_0 + H_{MAE},$$

$$H_0 = - \sum_{\langle i,j \rangle} J_1 \mathbf{S}_i \cdot \mathbf{S}_j - \sum_{\langle\langle i,j \rangle\rangle} J_2 \mathbf{S}_i \cdot \mathbf{S}_j - \sum_{\langle\langle\langle i,j \rangle\rangle\rangle} J_3 \mathbf{S}_i \cdot \mathbf{S}_j, \quad (1)$$

where H_0 is the isotropic Heisenberg model with J_1 , J_2 and J_3 the intralayer the first-, second-, and third-nearest-neighbor exchange interactions, respectively, and H_{MAE} is the magnetic anisotropy including the Kitaev-like exchange anisotropy and the single-ion

anisotropy [52, 53]. The calculation details are provided in Supplemental Materials. For the two adjacent layers sliding $\sqrt{3}/3a$ along the armchair direction, the interlayer interaction H_{inter} could be written as

$$H_{inter} = - \sum_{\langle i,i' \rangle} J_1' \mathbf{S}_i \cdot \mathbf{S}_{i'} - \sum_{\langle\langle i,i' \rangle\rangle} J_2' \mathbf{S}_i \cdot \mathbf{S}_{i'}, \quad (2)$$

where J_1' and J_2' are the interlayer first- and second-nearest-neighbor exchange interactions, respectively, and i and i' represent Cr atoms in the adjacent layers. While for the two adjacent layers sliding $1/3a$ along the zigzag direction, the interlayer interaction H_{inter} is written as

$$H_{inter} = - \sum_{\langle i,i' \rangle} J_1'' \mathbf{S}_i \cdot \mathbf{S}_{i'}, \quad (3)$$

where J_1'' represents the interlayer nearest exchange interactions. The exchange couplings existing in stacking structures I to IV are marked in Fig. 3. Because the interlayer exchange couplings are included in the model for the stacking structures of trilayer CrI_3 , the intralayer second and third nearest-neighbor exchange couplings J_2 and J_3 are also included, as discussed in subsection III.A. The values of J_1 , J_2 , J_3 , J_1' , J_2' and J_1'' can be extracted from DFT results by calculating the energies of several different spin configurations as shown in Figs. S2-S4 in Supplemental Materials, and the results for stacking structures I to IV under different strains are listed in Table II. By Eqs. (1) - (3), positive (negative) exchange integrals indicate a FM (AFM) interaction. When the applied strain is between -6%~10%, the calculated intralayer exchange couplings J_1 and J_2 are all positive values, which are much larger than that of J_3 which is negligible small. Table II and Fig. 2 show that J_1 is weakened and becomes a negative value when the compressive strain is larger than 6%. The intralayer nearest-neighbor exchange coupling is determined by the competition between AFM direct exchange and FM superexchange [54–56]. Decreasing Cr-Cr intralayer distance, the AFM direct exchange can be enhanced, and will dominate the intralayer exchange interaction.

D. Comparison with the experiment

Three different magnetic phases FM- $\uparrow\uparrow\uparrow$, FM- $\downarrow\uparrow\downarrow$, FM- $\uparrow\uparrow\downarrow$ have been experimentally observed in the trilayer CrI_3 under the application of pressure [43]. For the measured FM- $\downarrow\uparrow\downarrow$ magnetic phase, which corresponds to II (monoclinic) and III (hexagonal) stacking structures with a tiny tensile strain based on our DFT results, the critical field (B_C) polarizing the FM- $\downarrow\uparrow\downarrow$ state to FM- $\uparrow\uparrow\uparrow$ state under different pressure is reported in the experiment [43]. Here, we adopt $4J_1''|S|^2 \approx -g\mu_B S B_C$ to roughly estimate the strength of the interlayer exchange

TABLE II. The magnetic ground state, intralayer and interlayer exchange couplings (meV) and magnetic anisotropy energy (meV/Cr) under different strains for four stacking structures. J_1 , J_2 , J_3 , J'_1 , J'_2 and J''_1 are labeled in Fig. 3, and a positive value indicates ferromagnetic coupling, whereas a negative value indicates antiferromagnetic coupling. Positive value of E_{MAE} indicates the out-of-plane magnetization, otherwise the in-plane magnetization. The four stacking structures and different spin configurations are shown in Fig. 1.

Trilayer CrI ₃	Strain	Ground state	$J_1 S ^2$	$J_2 S ^2$	$J_3 S ^2$	$J'_1 S ^2$	$J'_2 S ^2$	$J''_1 S ^2$	E_{MAE}
I (rhombohedral)	-6%	FM- $\uparrow\uparrow\uparrow$	2.09	2.26	-0.89	-0.43	0.57	/	1.22
	0%	FM- $\uparrow\uparrow\uparrow$	9.14	1.51	-0.19	-0.57	0.67	/	0.63
	6%	FM- $\uparrow\uparrow\uparrow$	11.23	1.12	-0.05	-0.46	0.82	/	0.62
II(monoclinic)	-6%	FM- $\uparrow\uparrow\uparrow$	2.06	2.18	-0.70	/	/	0.13	1.22
	0%	FM- $\uparrow\uparrow\uparrow$	9.21	1.34	0.06	/	/	0.01	0.61
	6%	FM- $\downarrow\uparrow\downarrow$	11.18	1.02	0.14	/	/	-0.41	0.29
III(hexagonal)	-6%	FM- $\uparrow\uparrow\uparrow$	2.05	2.19	-0.70	/	/	0.14	1.25
	0%	FM- $\uparrow\uparrow\uparrow$	9.20	1.35	0.07	/	/	0.02	0.66
	6%	FM- $\downarrow\uparrow\downarrow$	11.18	1.02	0.13	/	/	-0.38	0.46
IV(triclinic)	-6%	FM- $\uparrow\uparrow\uparrow$	2.06	2.18	-0.69	-0.50	0.59	0.13	1.23
	0%	FM- $\uparrow\uparrow\uparrow$	9.28	1.33	0.06	-0.63	0.70	0.01	0.61
	6%	FM- $\uparrow\uparrow\downarrow$	11.20	1.01	0.13	-0.53	0.83	-0.39	0.45

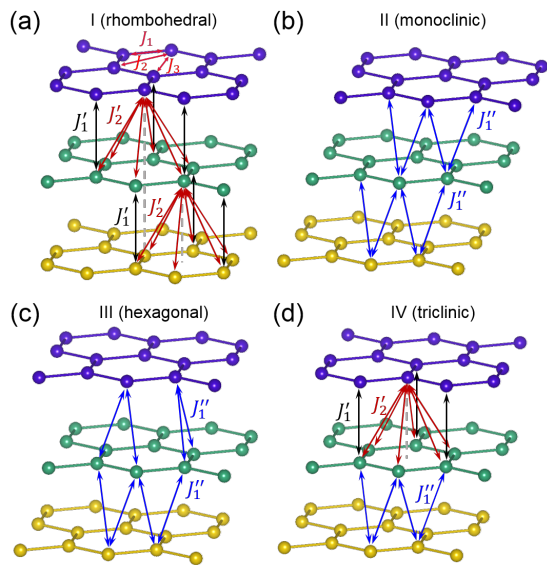


FIG. 3. Interlayer interactions in (a) I (rhombohedral) with the first (J'_1) and second (J'_2) nearest-neighboring exchange couplings labeled, (b) II (monoclinic) with the nearest-neighbor (J''_1) labeled, (c) III (hexagonal) with the nearest-neighbor (J''_1) labeled and (d) IV (triclinic) with J'_1 , J'_2 and J''_1 co-existing, respectively. The intralayer interactions including first (J_1), second (J_2) and third (J_3) nearest-neighboring exchange couplings between two Cr atoms are marked in (a).

coupling J''_1 under different pressures. The experimen-

tal values of B_C under 0 and 2.45 GPa are 1.6 and 3.7 T, respectively. Thus the corresponding interlayer exchange couplings $J''_1|S|^2$ could be obtained as -0.07 and -0.16 meV, respectively. The values of $J''_1|S|^2$ obtained from the DFT results for II (monoclinic) stacking structure are plotted as a function of the applied strain as shown in Fig. 4(a). In this way, for the applied pressure in the experiment, the corresponding tensile strain can be estimated. As noted in Fig. 4 (a), for the 0 GPa in the experiment, a small tensile strain about 1.4% is obtained in our estimation. The strain may be due to the existence of the encapsulation of trilayer CrI₃ by graphene and h-BN in the experimental setup [43]. The estimated strain is increased to 2.9% when the pressure is applied to 2.45 GPa in the experiment. For the measured FM- $\uparrow\uparrow\downarrow$ magnetic phase under 2.45 GPa pressure, which corresponds to IV (triclinic) stacking structure with tensile strain based on our DFT results, $2J''_1|S|^2 \approx -g\mu_B SB_C$ is used to estimate the value of $J''_1|S|^2$ and the result is marked in Fig. 4(b). Magnetic anisotropy energy (MAE) is calculated by the energy difference between states with out-of-plane and in-plane magnetization, as plotted in Fig. 4(c). It is found that the MAE is strongly dependent on the magnetic phase in trilayer CrI₃, and in the strain range of -6%~0%, the stacking structures I to IV possess the FM- $\uparrow\uparrow\uparrow$ state, and their MAE are almost the same and decrease with the increase of lattice constant. With the application of tensile strain, the magnetic phase of stacking structures I to IV becomes different, and the

values of their MAE are different.

The Curie temperatures T_C for II (monoclinic) and III (hexagonal) stacking structures in trilayer CrI_3 with FM- $\downarrow\uparrow\downarrow$ state are simulated by Monte Carlo (MC) simulation based on a Hamiltonian described in Eqs. (1) - (3). A $40 \times 40 \times 1$ supercell of hexagonal lattice with periodic boundary conditions is adopted, and the MC steps for each temperature is 10^6 . T_C as a function of applied strain is plotted in Fig. 4(d). According to our calculations, in both monolayer and trilayer CrI_3 , the multiples of experimental T_C and simulated T_C are close to 0.58 (see Supplemental Materials). Thus, to avoid the problem of overestimating T_C in theoretical studies and better compare with the experimental results, the T_C value obtained from the MC simulation for trilayer CrI_3 in our calculations are all rescaled by a factor of 0.58 to reproduce the experimental result. It is noted that the rescaled T_C increases with the increase of tensile stain for small strain, which is qualitatively consistent with the experimental observation of T_C [43].

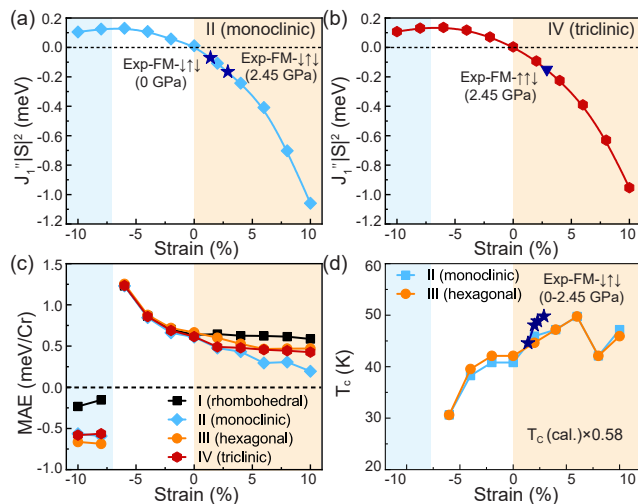


FIG. 4. Strain dependent interlayer exchange coupling $J'_{||} |S|^2$ for (a) monoclinic and (b) triclinic stacking orders. The navy blue points are simulated from the experimental results [43]. (c) Strain-dependent magnetic anisotropy energy (MAE) which is defined as $E_{m||x} - E_{m||z}$ for four different stacking structures in trilayer CrI_3 . A positive value of MAE indicates the out-of-plane magnetization, otherwise the in-plane magnetization. (d) Strain-dependent Curie temperature (T_C) for II (monoclinic) and III (hexagonal) stacking structures in trilayer CrI_3 by Monte Carlo simulations, which has been rescaled by a factor of 0.58 to reproduce the experimental results. The navy blue points in (d) are the experimental T_C in trilayer CrI_3 with different applied pressures [43].

E. Effect of electronic correlation

For $3d$ orbitals in transitions-metal compounds, the electronic correlation parameter U is important, and the estimated value for Cr atom in CrI_3 via the linear response approach [57] is about 3.35 eV (see Supplemental Materials). Thus, $U = 3$ eV is adopted in our above DFT calculations. To verify the robustness of our DFT results, we have also studied the magnetic phases of the four stacking structures under different strains with $U = 4$ eV. It is shown that our conclusion does not change for $U = 3$ and 4 eV. As shown in Fig. S8 in Supplemental Materials, for all four stacking structures, by applying a small tensile strain, the FM- $\uparrow\uparrow\uparrow$ magnetic state remains for I (rhombohedral) stacking structure, while it changes to FM- $\downarrow\uparrow\downarrow$ for II (monoclinic) and III (hexagonal) stacking structures, and it transforms to FM- $\uparrow\uparrow\downarrow$ for IV (triclinic) stacking structure. So, our conclusions do not change for reasonable parameter range of $U = 3 \sim 4$ eV. In addition, for the DFT+ U scheme with U ranging from 0 to 4 eV, the picture of $S=3/2$ with all spin up t_{2g} orbitals occupied is reasonable (see Fig. S2 in Supplemental Materials). The crystal-field splitting between t_{2g} and e_g orbitals of the trilayer CrI_3 with I (rhombohedral) stacking order can be roughly estimated as 3.62 eV, which changes slightly with the strain (see Fig. S3 in Supplemental Materials).

VI. CONCLUSION

In summary, by using the first-principles calculations, we find that the magnetic states in trilayer CrI_3 strongly depend on the stacking structures and interlayer distance. All four different stacking structures, including I (rhombohedral), II (monoclinic), III (hexagonal) and IV (triclinic), the FM- $\uparrow\uparrow\uparrow$ is the magnetic ground state. Under a small tensile strain, FM- $\uparrow\uparrow\uparrow$ is maintained in I (rhombohedral), while it transforms to FM- $\downarrow\uparrow\downarrow$ for II (monoclinic) and III (hexagonal), and changes to FM- $\uparrow\uparrow\downarrow$ for IV (triclinic). The three obtained magnetic states are consistent with the observations in the recent experiment. The intralayer and interlayer exchange couplings are extracted based on a Heisenberg-type Hamiltonian, which can well interpret the change of magnetic behavior in trilayer CrI_3 . Our results also show that the band gap and MAE of trilayer CrI_3 are strongly dependent on the magnetic phases. This study presents a reasonable explanation for the experimental observations for the trilayer CrI_3 , and paves a way to design multilayer devices with desired properties, such as novel magnetic states, suitable band gaps, and so on.

ACKNOWLEDGEMENTS

This work is supported in part by the National Key R&D Program of China (Grant No. 2018YFA0305800), the Strategic Priority Research Program of the Chinese Academy of Sciences (Grant No. XDB28000000), the National Natural Science Foundation of China (Grant No. 11834014), and Beijing Municipal Science and Technology Commission (Grant No. Z191100007219013). B.G. is also supported by the National Natural Science Foundation of China (Grants No. Y81Z01A1A9 and No. 12074378), the Chinese Academy of Sciences (Grants No. YSBR-030, No. Y929013EA2 and No. E0EG4301X2), the University of Chinese Academy of Sciences (Grant No. 110200M208), the Strategic Priority Research Program of Chinese Academy of Sciences (Grant No. XDB33000000), and the Beijing Natural Science Foundation (Grant No. Z190011).

* phyjyy@nus.edu.sg

† gubo@ucas.ac.cn

‡ gsu@ucas.ac.cn

- [1] B. Huang, G. Clark, E. Navarro-Moratalla, D. R. Klein, R. Cheng, K. L. Seyler, D. Zhong, E. Schmidgall, M. A. McGuire, D. H. Cobden, W. Yao, D. Xiao, P. Jarillo-Herrero, and X. Xu, Layer-dependent ferromagnetism in a van der Waals crystal down to the monolayer limit, *Nature* **546**, 270 (2017).
- [2] C. Gong, L. Li, Z. Li, H. Ji, A. Stern, Y. Xia, T. Cao, W. Bao, C. Wang, Y. Wang, Z. Q. Qiu, R. J. Cava, S. G. Louie, J. Xia, and X. Zhang, Discovery of intrinsic ferromagnetism in two-dimensional van der Waals crystals, *Nature* **546**, 265 (2017).
- [3] M. Gibertini, M. Koperski, A. F. Morpurgo, and K. S. Novoselov, Magnetic 2D materials and heterostructures, *Nat. Nanotechnol.* **14**, 408 (2019).
- [4] J.-Y. You, C. Chen, Z. Zhang, X.-L. Sheng, S. A. Yang, and G. Su, Two-dimensional weyl half-semimetal and tunable quantum anomalous hall effect, *Phys. Rev. B* **100**, 064408 (2019).
- [5] J.-Y. You, Z. Zhang, B. Gu, and G. Su, Two-dimensional room-temperature ferromagnetic semiconductors with quantum anomalous hall effect, *Phys. Rev. Applied* **12**, 024063 (2019).
- [6] V. P. Ningrum, B. Liu, W. Wang, Y. Yin, Y. Cao, C. Zha, H. Xie, X. Jiang, Y. Sun, S. Qin, X. Chen, T. Qin, C. Zhu, L. Wang, and W. Huang, Recent advances in two-dimensional magnets: Physics and devices towards spintronic applications, *Research* **2020**, 1 (2020).
- [7] J.-Y. You, B. Gu, and G. Su, P-orbital magnetic topological states on square lattice, *Natl. Sci. Rev.* **10.1093/nsr/nwab114** (2021).
- [8] N. D. Mermin and H. Wagner, Absence of ferromagnetism or antiferromagnetism in one- or two-dimensional isotropic Heisenberg models, *Phys. Rev. Lett.* **17**, 1133 (1966).
- [9] J.-Y. You, Z. Zhang, X.-J. Dong, B. Gu, and G. Su, Two-dimensional magnetic semiconductors with room Curie temperatures, *Phys. Rev. Research* **2**, 013002 (2020).
- [10] Y. Deng, Y. Yu, Y. Song, J. Zhang, N. Z. Wang, Z. Sun, Y. Yi, Y. Z. Wu, S. Wu, J. Zhu, J. Wang, X. H. Chen, and Y. Zhang, Gate-tunable room-temperature ferromagnetism in two-dimensional Fe₃GeTe₂, *Nature* **563**, 94 (2018).
- [11] M. Bonilla, S. Kolekar, Y. Ma, H. C. Diaz, V. Kalappattil, R. Das, T. Eggers, H. R. Gutierrez, M.-H. Phan, and M. Batzill, Strong room-temperature ferromagnetism in VSe₂ monolayers on van der waals substrates, *Nat. Nanotechnol.* **13**, 289 (2018).
- [12] D. J. O'Hara, T. Zhu, A. H. Trout, A. S. Ahmed, Y. K. Luo, C. H. Lee, M. R. Brenner, S. Rajan, J. A. Gupta, D. W. McComb, and R. K. Kawakami, Room temperature intrinsic ferromagnetism in epitaxial manganese selenide films in the monolayer limit, *Nano Lett.* **18**, 3125 (2018).
- [13] M. Weisheit, S. Fahler, A. Marty, Y. Souche, C. Poinson, and D. Givord, Electric field-induced modification of magnetism in thin-film ferromagnets, *Science* **315**, 349 (2007).
- [14] Z. Zhang, J.-Y. You, B. Gu, and G. Su, Antiferromagnetic and electric polarized states in two-dimensional janus semiconductor Fe₂Cl₃I₃, *J. Phys. Chem. C* **124**, 19219 (2020).
- [15] J.-Y. You, X.-J. Dong, B. Gu, and G. Su, Electric field induced topological phase transition and large enhancements of spin-orbit coupling and curie temperature in two-dimensional ferromagnetic semiconductors, *Phys. Rev. B* **103**, 104403 (2021).
- [16] T. Mukherjee, S. Chowdhury, D. Jana, and L. C. L. Y. Voon, Strain induced electronic and magnetic properties of 2D magnet CrI₃: a DFT approach, *J. Phys.: Condens. Matter* **31**, 335802 (2019).
- [17] X.-J. Dong, J.-Y. You, B. Gu, and G. Su, Strain-induced room-temperature ferromagnetic semiconductors with large anomalous hall conductivity in two-dimensional Cr₂Ge₂Se₆, *Phys. Rev. Applied* **12**, 014020 (2019).
- [18] W. Chen, Z. Sun, Z. Wang, L. Gu, X. Xu, S. Wu, and C. Gao, Direct observation of van der waals stacking dependent interlayer magnetism, *Science* **366**, 983 (2019).
- [19] D. Zhong, K. L. Seyler, X. Linpeng, R. Cheng, N. Sivadas, B. Huang, E. Schmidgall, T. Taniguchi, K. Watanabe, M. A. McGuire, W. Yao, D. Xiao, K.-M. C. Fu, and X. Xu, Van der waals engineering of ferromagnetic semiconductor heterostructures for spin and valleytronics, *Sci. Adv.* **3**, e1603113 (2017).
- [20] M. Mogi, A. Tsukazaki, Y. Kaneko, R. Yoshimi, K. S. Takahashi, M. Kawasaki, and Y. Tokura, Ferromagnetic insulator Cr₂Ge₂Te₆ thin films with perpendicular remanence, *APL Materials* **6**, 091104 (2018).
- [21] H. Wang, Y. Liu, P. Wu, W. Hou, Y. Jiang, X. Li, C. Pandey, D. Chen, Q. Yang, H. Wang, D. Wei, N. Lei, W. Kang, L. Wen, T. Nie, W. Zhao, and K. L. Wang, Above room-temperature ferromagnetism in wafer-scale two-dimensional van der waals Fe₃GeTe₂ tailored by a topological insulator, *ACS Nano* **14**, 10045 (2020).
- [22] X.-J. Dong, J.-Y. You, Z. Zhang, B. Gu, and G. Su, Great enhancement of curie temperature and magnetic anisotropy in two-dimensional van der waals magnetic semiconductor heterostructures, *Phys. Rev. B* **102**, 144443 (2020).
- [23] Y. Deng, Y. Yu, M. Z. Shi, Z. Guo, Z. Xu, J. Wang, X. H. Chen, and Y. Zhang, Quantum anomalous hall effect in

- intrinsic magnetic topological insulator MnBi_2Te_4 , *Science* **367**, 895 (2020).
- [24] Y.-F. Zhao, R. Zhang, R. Mei, L.-J. Zhou, H. Yi, Y.-Q. Zhang, J. Yu, R. Xiao, K. Wang, N. Samarth, M. H. W. Chan, C.-X. Liu, and C.-Z. Chang, Tuning the chern number in quantum anomalous hall insulators, *Nature* **588**, 419 (2020).
- [25] C. Liu, Y. Wang, H. Li, Y. Wu, Y. Li, J. Li, K. He, Y. Xu, J. Zhang, and Y. Wang, Robust axion insulator and chern insulator phases in a two-dimensional antiferromagnetic topological insulator, *Nat. Mater.* **19**, 522 (2020).
- [26] T. Song, X. Cai, M. W.-Y. Tu, X. Zhang, B. Huang, N. P. Wilson, K. L. Seyler, L. Zhu, T. Taniguchi, K. Watanabe, M. A. McGuire, D. H. Cobden, D. Xiao, W. Yao, and X. Xu, Giant tunneling magnetoresistance in spin-filter van der waals heterostructures, *Science* **360**, 1214 (2018).
- [27] Z. Wang, I. Gutiérrez-Lezama, N. Ubrig, M. Kroner, M. Gibertini, T. Taniguchi, K. Watanabe, A. Imamoğlu, E. Giannini, and A. F. Morpurgo, Very large tunneling magnetoresistance in layered magnetic semiconductor CrI_3 , *Nat. Commun.* **9**, 2516 (2018).
- [28] D. R. Klein, D. MacNeill, J. L. Lado, D. Soriano, E. Navarro-Moratalla, K. Watanabe, T. Taniguchi, S. Manni, P. Canfield, J. Fernández-Rossier, and P. Jarillo-Herrero, Probing magnetism in 2D van der waals crystalline insulators via electron tunneling, *Science* **360**, 1218 (2018).
- [29] H. H. Kim, B. Yang, T. Patel, F. Sfigakis, C. Li, S. Tian, H. Lei, and A. W. Tsien, One million percent tunnel magnetoresistance in a magnetic van der waals heterostructure, *Nano Lett.* **18**, 4885 (2018).
- [30] N. Sivadas, S. Okamoto, X. Xu, C. J. Fennie, and D. Xiao, Stacking-dependent magnetism in bilayer CrI_3 , *Nano Lett.* **18**, 7658 (2018).
- [31] P. Jiang, C. Wang, D. Chen, Z. Zhong, Z. Yuan, Z.-Y. Lu, and W. Ji, Stacking tunable interlayer magnetism in bilayer CrI_3 , *Phys. Rev. B* **99**, 144401 (2019).
- [32] S. W. Jang, M. Y. Jeong, H. Yoon, S. Rye, and M. J. Han, Microscopic understanding of magnetic interactions in bilayer CrI_3 , *Phys. Rev. Materials* **3**, 031001 (2019).
- [33] Z. Sun, Y. Yi, T. Song, G. Clark, B. Huang, Y. Shan, S. Wu, D. Huang, C. Gao, Z. Chen, M. McGuire, T. Cao, D. Xiao, W.-T. Liu, W. Yao, X. Xu, and S. Wu, Giant nonreciprocal second-harmonic generation from antiferromagnetic bilayer CrI_3 , *Nature* **572**, 497 (2019).
- [34] K. Guo, B. Deng, Z. Liu, C. Gao, Z. Shi, L. Bi, L. Zhang, H. Lu, P. Zhou, L. Zhang, Y. Cheng, and B. Peng, Layer dependence of stacking order in nonencapsulated few-layer CrI_3 , *Sci. China Mater.* **63**, 413 (2019).
- [35] A. M. León, J. W. González, J. Mejía-López, F. C. de Lima, and E. S. Morell, Strain-induced phase transition in CrI_3 bilayers, *2D Mater.* **7**, 035008 (2020).
- [36] C. Lei, B. L. Chittari, K. Nomura, N. Banerjee, J. Jung, and A. H. MacDonald, Magnetoelectric response of antiferromagnetic CrI_3 bilayers, *Nano Lett.* **21**, 1948 (2021).
- [37] H. Tian, C. Xu, X. Li, Y. Yang, L. Bellaiche, and D. Wu, Band structure engineering of van der waals heterostructures using ferroelectric clamped sandwich structures, *Phys. Rev. B* **103**, 125426 (2021).
- [38] F. Cantos-Prieto, A. Falin, M. Alliat, D. Qian, R. Zhang, T. Tao, M. R. Barnett, E. J. G. Santos, L. H. Li, and E. Navarro-Moratalla, Layer-dependent mechanical properties and enhanced plasticity in the van der waals chromium trihalide magnets, *Nano Lett.* [10.1021/acs.nanolett.0c04794](https://doi.org/10.1021/acs.nanolett.0c04794) (2021).
- [39] S. Jiang, J. Shan, and K. F. Mak, Electric-field switching of two-dimensional van der waals magnets, *Nat. Mater.* **17**, 406 (2018).
- [40] S. Jiang, L. Li, Z. Wang, K. F. Mak, and J. Shan, Controlling magnetism in 2D CrI_3 by electrostatic doping, *Nat. Nanotechnol.* **13**, 549 (2018).
- [41] B. Huang, G. Clark, D. R. Klein, D. MacNeill, E. Navarro-Moratalla, K. L. Seyler, N. Wilson, M. A. McGuire, D. H. Cobden, D. Xiao, W. Yao, P. Jarillo-Herrero, and X. Xu, Electrical control of 2D magnetism in bilayer CrI_3 , *Nat. Nanotechnol.* **13**, 544 (2018).
- [42] T. Li, S. Jiang, N. Sivadas, Z. Wang, Y. Xu, D. Weber, J. E. Goldberger, K. Watanabe, T. Taniguchi, C. J. Fennie, K. F. Mak, and J. Shan, Pressure-controlled interlayer magnetism in atomically thin CrI_3 , *Nat. Mater.* **18**, 1303 (2019).
- [43] T. Song, Z. Fei, M. Yankowitz, Z. Lin, Q. Jiang, K. Hwangbo, Q. Zhang, B. Sun, T. Taniguchi, K. Watanabe, M. A. McGuire, D. Graf, T. Cao, J.-H. Chu, D. H. Cobden, C. R. Dean, D. Xiao, and X. Xu, Switching 2D magnetic states via pressure tuning of layer stacking, *Nat. Mater.* **18**, 1298 (2019).
- [44] J. F. Dillon and C. E. Olson, Magnetization, resonance, and optical properties of the ferromagnet CrI_3 , *J. Appl. Phys.* **36**, 1259 (1965).
- [45] M. A. McGuire, H. Dixit, V. R. Cooper, and B. C. Sales, Coupling of crystal structure and magnetism in the layered, ferromagnetic insulator CrI_3 , *Chem. Mater.* **27**, 612 (2015).
- [46] P. E. Blöchl, Projector augmented-wave method, *Phys. Rev. B* **50**, 17953 (1994).
- [47] G. Kresse and J. Hafner, Ab initio molecular dynamics for liquid metals, *Phys. Rev. B* **47**, 558 (1993).
- [48] G. Kresse and J. Furthmüller, Efficient iterative schemes for ab initio total-energy calculations using a plane-wave basis set, *Phys. Rev. B* **54**, 11169 (1996).
- [49] J. P. Perdew, K. Burke, and M. Ernzerhof, Generalized gradient approximation made simple, *Phys. Rev. Lett.* **77**, 3865 (1996).
- [50] H. J. Monkhorst and J. D. Pack, Special points for brillouin-zone integrations, *Phys. Rev. B* **13**, 5188 (1976).
- [51] L. Webster and J.-A. Yan, Strain-tunable magnetic anisotropy in monolayer CrCl_3 , CrBr_3 , and CrI_3 , *Phys. Rev. B* **98**, 144411 (2018).
- [52] H. Xiang, C. Lee, H.-J. Koo, X. Gong, and M.-H. Whangbo, Magnetic properties and energy-mapping analysis, *Dalton Trans.* **42**, 823 (2013).
- [53] C. Xu, J. Feng, H. Xiang, and L. Bellaiche, Interplay between kitaev interaction and single ion anisotropy in ferromagnetic CrI_3 and CrGeTe_3 monolayers, *npj Comput. Mater.* **4**, 57 (2018).
- [54] J. B. Goodenough, An interpretation of the magnetic properties of the perovskite-type mixed crystals $\text{La}_{1-x}\text{Sr}_x\text{CoO}_{3-\lambda}$, *J. Phys. Chem. Solids* **6**, 287 (1958).
- [55] J. Kanamori, Superexchange interaction and symmetry properties of electron orbitals, *J. Phys. Chem. Solids* **10**, 87 (1959).
- [56] J. L. Lado and J. Fernández-Rossier, On the origin of magnetic anisotropy in two dimensional CrI_3 , *2D Mater.* **4**, 035002 (2017).
- [57] M. Cococcioni and S. de Gironcoli, Linear response approach to the calculation of the effective interaction parameters in the LDA+U method, *Phys. Rev. B* **71**,

035105 (2005).